Available online at www.sciencedirect.com
SCIENCE DIRECT®
Journal of Sound and Vibration 275 (2004) 127–149
JOURNAL OF SOUND AND VIBRATION
www.elsevier.com/locate/jsvi

A novel approach to the calculation of pothole-induced contact forces in MDOF vehicle models

A.V. Pesterev[a], L.A. Bergman[b], C.A. Tan[c,*]

[a] *Institute for Systems Analysis, Russian Academy of Sciences, pr. 60-letiya Oktyabrya 9, Moscow 117312, Russia*
[b] *Aeronautical and Astronautical Engineering Department, University of Illinois at Urbana-Champaign, 104 S. Wright St., Urbana, IL 61801, USA*
[c] *Department of Mechanical Engineering, Wayne State University, 5050 Anthony Wayne Drive, Detroit, MI 48202, USA*

Received 20 May 2002; accepted 18 June 2003

Abstract

A technique is developed to predict the dynamic contact forces arising after passing road surface irregularities by a vehicle modelled as an undamped multiple-degrees-of-freedom (MDOF) system. An MDOF system moving along an uneven profile is decomposed into an aggregate of independent oscillators in the modal space, such that the response of each oscillator can be calculated independently. An equation relating the contact forces in the physical space to the modal forces is established. The technique developed is applied to the calculation of the coefficients of the harmonic components of the contact forces arising after the passage of a "cosine" pothole. The application of the technique to various problems, such as evaluation of the effect of parameter modifications on the vehicle dynamics and reduction of vehicle models in bridge-related problems, as well as its extension to the damped case, are also discussed. One interesting phenomenon reported in the DIVINE project [1], regarding the replacement of a steel suspension by an air suspension, resulting in an increase of the maximum response of short-span bridges, is explained by applying the technique suggested. The discussion is amply illustrated by examples of the application of the technique to the calculation of the tire forces due to a pothole for two simple—quarter-car and half-car—vehicle models.

1. Introduction

The paper is concerned with the assessment of dynamic tire forces that arise after the passage of a road surface irregularity by a vehicle. This problem is of great importance as it is well known that dynamic loads produced by vehicles considerably affect damage of the infrastructure

*Corresponding author. Tel.: +1-313-577-3888; fax: +1-313-578-5932.
E-mail address: tan@wayne.edu (C.A. Tan).

0022-460X/$ - see front matter © 2003 Elsevier Ltd. All rights reserved.
doi:10.1016/S0022-460X(03)00789-2

(pavement or bridges), a significant portion of which in many countries is either aging or reaching the end of its life. The recently concluded multinational DIVINE (Dynamic Interaction Between Vehicles and Infrastructure Experiment) project [1] indicates that trucks "wear" pavements at a rate which is dependent not only on the static load carried by the vehicle, but also on the dynamic performance of the vehicle, on the longitudinal profile of the road and on the structural variability of the pavement. The outcomes of this project suggest that current understanding of the dynamic interactions between moving vehicles and the infrastructure carrying them is inadequate.

This study originated from our earlier works on the examination of vibration of bridges traversed by heavy vehicles and was motivated by results of field and numerical experiments reported in some publications (e.g., Refs. [1–3]) that showed large values (more than 100%) of the dynamic increment (in some publications, dynamic load factor (DLF)), defined as [2]

$$DI = \frac{(\delta_{dyn} - \delta_{static})}{\delta_{static}} \times 100\%,$$

where δ_{dyn} and δ_{static} are peak dynamic and static deflections, respectively. Such large values of the DI cannot be explained in the framework of simple—moving force or moving mass—vehicle models. Indeed, the dependence of the maximum deflection of a simply supported beam on the speed of the traveling force presented in Ref. [4] shows that the maximum DI (about 70%) occurs at very high speed and, for the vehicle speeds of interest, it does not exceed 10–15%. The inertia effect of the moving mass in this speed range is also small and can be neglected. Moreover, as can be concluded from many publications, as well as from our numerical experiments, such large values of the DI cannot be obtained in the framework of more complicated—multiple-degrees-of-freedom models if the bridge surface is assumed to have a flat longitudinal profile (as noted in Ref. [1], "for a smooth profile, the influence of the truck suspension is insignificant"). The above arguments lead us to speculate that the *large values of the DI measured in some field experiments can be explained only by the presence of road irregularities on the bridge and its approaches*. Then it follows that the examination of the effect of an uneven road profile is crucial in the analysis of high-magnitude bridge vibration.

The effect of road surface irregularities on the bridge vibration has been examined by many researchers (see, e.g., Refs. [1–3,5–8] and references therein), and many methods for numerically solving the problem of a vehicle moving along a bridge with an uneven surface have been developed (e.g., Refs. [6–11]). The main difficulty associated with this problem is in the large number of parameters involved. As a result, the majority of studies reported in the literature are confined to extensive numerical modelling or field experiments. An obvious disadvantage of these approaches is that results of numerical or field experiments are often valid only for a particular bridge and vehicle and cannot easily be generalized to other configurations. It is then not surprising that results reported in the literature are sometimes contradictory. This point is well illustrated by the following examples. In both Refs. [2] and [5], short-span bridges are considered. However, Ref. [2] shows large values of the dynamic increment measured in field experiments (up to 137%), whereas, Ref. [5] reports that "the analytical simulations and field tests showed that DLF is considerably lower than code-specified values" (the latter are around 30% depending on the code and bridge length) and recommends to reduce the design values of DLF. Another example of this kind can be found in Ref. [3]. The authors explore how different factors influence bridge behavior. Based on results of numerical experiments with elaborate finite-dimensional

models of a bridge and vehicle, they conclude that, in terms of the maximum bridge deflection, the "initial vehicle suspension oscillation had the greatest effect" and the "bridge-surface roughness was found to have negligible effect". On the other hand, they justly note that road surface irregularities on the bridge approaches is the principal cause of the initial suspension oscillation, which means, in fact, that it is road roughness (road surface irregularities) that had the greatest effect on the maximum bridge deflection.

In view of complexity of the problem of coupled bridge–vehicle vibration associated with a large number of parameters affecting the solution in a non-trivial way, it is advisable to start examination from certain typical isolated (local) irregularities. Moreover, it is important, in our opinion, to examine first the problem of finding the vehicle response due to the passage of an irregularity located on the rigid foundation. To justify this point, we note that the local character of an irregularity suggests shortness of the passage time and, in view of the considerable inertia of the bridge, its dynamics cannot be noticeably changed during that time. In addition, analysis of results of field and numerical experiments reported in the literature, as well as our numerical experiments, show that dynamic contact forces arising when a vehicle passes typical road surface irregularities are considerably greater than those caused by coupled bridge–vehicle vibration in the case of an ideally smooth road surface. Hence, neglecting the bridge dynamics, we find adequate approximations of the additional vehicle oscillations and dynamic forces that arise during, or immediately after, the passage of a road surface irregularity. The effect of these additional forces on the bridge dynamics depends on the frequencies and magnitudes of these forces. Thus, in order to predict the effect of an irregularity on the bridge vibration, we basically need to know whether the frequency spectrum of the vehicle oscillations due to the irregularity contains frequencies that match the fundamental frequency of the bridge and whether the magnitudes of the corresponding harmonic forces are sizeable.

The problem of calculation of the dynamic forces arising after passing an irregularity is very important also in studies related to pavement damage [1,12–16]. Based on experimental results reported in the literature, Potter et al. [12] conclude that the peak damage due to dynamic loads can be between 1.5 and 12 times the level of damage caused by a static load and note that, at highway speeds, "the parameter which causes the greatest variation in dynamic tyre forces, and the largest changes in ranking of suspensions, is the road roughness level." Moreover, as indicated in Ref. [14], there is evidence that "fatigue failure of pavements is likely to be governed by peak dynamic forces, and not by the average dynamic forces." Then it follows that, both in bridge and pavement damage-related applications, it is critically important to establish dependence of the peak tire forces arising after passing an irregularity on the irregularity parameters, suspension characteristics, and vehicle speed.

The general idea of the approach discussed in this paper is to decouple equations governing vibration of an MDOF vehicle model moving along uneven road, to solve the uncoupled equations in the modal space, and to transform back the results obtained into the physical space. The fact that the model is decomposed into independent single-degree-of-freedom (SDOF) oscillators makes it possible to find solution for each oscillator analytically (or semi-analytically). The crucial step, when transforming back to the physical space, is to calculate not the contact forces themselves but rather the Fourier coefficients of their harmonic components. This allows us to represent the results obtained in a form suitable for subsequent analysis. Moreover, in many cases (e.g., when applied to problems of bridge vibration), the Fourier coefficients of the harmonic

components of the contact forces give us more valuable information than just magnitudes of the total dynamic forces.

In this paper, we consider the case of undamped vehicle models, although the approach discussed is applicable to damped vehicles as well (see Section 5.2). The format of the presentation is as follows. In Section 2, we reduce the problem of vibration of an MDOF vehicle moving along an uneven road to that of independent SDOF oscillators in the modal space. A technique for the calculation of contact forces arising after the passage of an isolated "cosine" pothole is presented in Section 3. In Section 4, an interesting phenomenon reported in Refs. [1,2] is discussed and explained by applying the technique suggested. Section 5 discusses extensions of the approach suggested to damped vehicle models, to local irregularities of different types, and to bridge-related problems.

To conclude the introduction, let us cite the DIVINE report [1]: "There is now a need for a higher level of scientific knowledge about the interaction between trucks and pavements, and between trucks and bridges, in order to introduce regulations based on vehicle performance in terms of road friendliness." It is achieving this goal that the work presented is aimed at.

2. Decomposition of MDOF vehicle model moving along an uneven road

Consider an undamped MDOF vehicle model with n degrees of freedom and m contact points, schematically shown in Fig. 1. Let $z(t) \in \mathbb{R}^n$ be a vector of its physical co-ordinates such that $z(t) = 0$ corresponds to the equilibrium state (the springs are loaded by the vehicle weight) and $z_{cont} \in \mathbb{R}^m$ be a vector of vehicle co-ordinates (in the general case, linear combinations of the co-ordinates) that take part in the interaction with the ground. Denote by l_i, $i = 1, \ldots, m$, the distance between the first and ith contact points such that $l_1 = 0$ and $l_{i+1} - l_i$ is the distance between the $(i+1)$th and ith contact points (distance between two adjacent axles). Let M be the mass matrix and $\bar{K}$ be stiffness matrix of the free-free (i.e., without the springs connected to the ground) vehicle. Denote by S_v the $m \times n$ matrix ("sensor" operator) that "chooses" contact

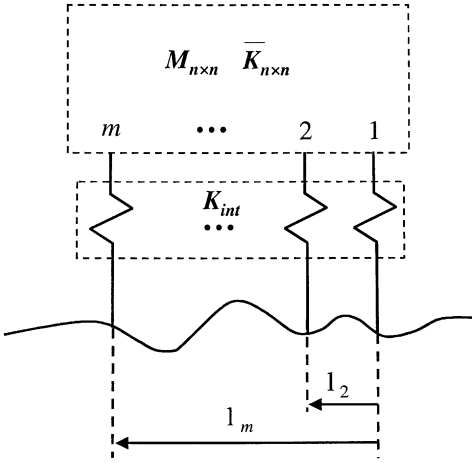

Fig. 1. A schematic of an MDOF vehicle moving along uneven profile.

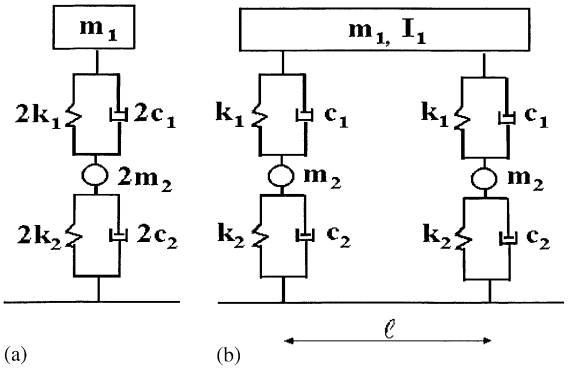

Fig. 2. (a) 2-DOF and (b) 4-DOF vehicle models.

co-ordinates, $z_{cont} = S_v z$, and by K_{int} a symmetric $m \times m$ matrix describing the interaction of the vehicle with the ground.

To exemplify the above notation, let us consider the "quarter-car" and "half-car" models depicted in Fig. 2. For the "quarter-car" model (Fig. 2(a)), we have

$$n = 2,\ m = 1,\ l_1 = 0,\ K_{int} = 2k_2,\ S_v = [0, 1].$$

For the "half-car" model (Fig. 2(b)), the parameters are

$$n = 4,\ m = 2,\ l_1 = 0,\ l_2 = l,\ K_{int} = \begin{bmatrix} k_2 & 0 \\ 0 & k_2 \end{bmatrix},\ S_v = \begin{bmatrix} 0 & 0 & 1 & 0 \\ 0 & 0 & 0 & 1 \end{bmatrix}.$$

The vehicle mass and stiffness matrices are written in a standard way and not presented here. The order of numbering the co-ordinates can be easily understood from the form of the matrices S_v.

The free vertical vibration of the vehicle resting on the rigid foundation is governed by the equation

$$M\ddot{z}(t) + \bar{K}z(t) = -S_v^{\mathrm{T}} K_{int} S_v z(t). \tag{1}$$

By introducing the notation

$$K = \bar{K} + S_v^{\mathrm{T}} K_{int} S_v \tag{2}$$

for the stiffness matrix of the supported vehicle, Eq. (1) reduces to

$$M\ddot{z}(t) + Kz(t) = 0. \tag{3}$$

Let now the vehicle move with a speed v along a road with a longitudinal profile $r(x)$. In this case, the vehicle is subject to external forces acting on it at the contact points due to variation in the road profile $r(x)$. Introduce the notation S_r for the operator defined by the relation

$$S_r r(x) = \begin{Bmatrix} r(x - l_1) \\ r(x - l_2) \\ \vdots \\ r(x - l_m) \end{Bmatrix}. \tag{4}$$

Then, it can be checked directly that the equation governing vertical vibration of the moving vehicle is given by

$$M\ddot{z}(t) + Kz(t) = S_v^{\mathrm{T}} K_{int} S_r r(vt). \tag{5}$$

Solving Eq. (3), we find vehicle eigenfrequencies ω_i ($f_i = \omega_i/2\pi$), $i = 1, \ldots, n$ (note that they all are non-zero since K is the stiffness matrix of the supported vehicle) and the matrix of vehicle eigenvectors ϕ. Representing z as $z(t) = \phi\eta(t)$, where η is a vector of modal co-ordinates, and multiplying both sides of Eq. (5) by ϕ^{T} from the left, we get the uncoupled equations in the modal co-ordinates,

$$\tilde{M}\ddot{\eta} + \tilde{K}\eta = \phi^{\mathrm{T}} S_v^{\mathrm{T}} K_{int} S_r r(vt), \tag{6}$$

where $\tilde{M} = \phi^{\mathrm{T}} M \phi \equiv \mathrm{diag}[\tilde{m}_i]$ and $\tilde{K} = \phi^{\mathrm{T}} K \phi \equiv \mathrm{diag}[\tilde{k}_i]$ are diagonal matrices.

Introducing the notation

$$A = \tilde{K}^{-1} \phi^{\mathrm{T}} S_v^{\mathrm{T}} K_{int} \tag{7}$$

and

$$\tilde{r}(x) = A S_r r(x), \tag{8}$$

where A is a dimensionless $n \times m$ matrix, we rewrite Eq. (6) in the form

$$\tilde{M}\ddot{\eta} + \tilde{K}\eta = \tilde{K}\tilde{r}(vt), \tag{9}$$

or, in a scalar form,

$$\tilde{m}_i \ddot{\eta}_i = -\tilde{k}_i(\eta_i - \tilde{r}_i(vt)), \quad i = 1, \ldots, n, \tag{10}$$

where $\tilde{r}_i$ is the ith component of the vector $\tilde{r}$.

Remark 1. Note that the case where the vehicle traverses a beam with an uneven profile $r(x)$ is treated in exactly the same way. In this case, the function $r(x)$ in all equations is to be replaced by $w(x, t) + r(x)$, where $w(x, t)$ is the displacement of the beam point x at time t.

As can be easily seen, the ith equation in Eq. (10) governs vibration of the SDOF oscillator with the modal mass $\tilde{m}_i$ and the spring coefficient $\tilde{k}_i$ moving along the profile $\tilde{r}_i(x)$. The matrix A transforms the input profile for the original MDOF vehicle model into the profiles $\tilde{r}_i(x)$ for the independent oscillators and is further referred to as the *model scaling matrix*. Thus, we reduced the problem of an MDOF system moving along a profile $r(x)$ to n independent problems for SDOF oscillators, with the profiles $\tilde{r}_i(x)$ being different for each oscillator. Solving n independent equations (10), we find the vector of modal co-ordinates η.

To derive a relationship between the vector of the dynamic contact (tire) forces

$$F_c(t) = K_{int}[S_v z(t) - S_r r(vt)] \tag{11}$$

and the modal force vector $\tilde{F}(t) = \tilde{K}(\eta(t) - \tilde{r}(vt))$, we take advantage of the following result.

Lemma 1. *For any linear vehicle model, the following matrix identity holds*:

$$A^{\mathrm{T}}\tilde{K}A \equiv K_{int}. \tag{12}$$

The lemma can be proved by considering conditions of static equilibrium for an MDOF vehicle resting on a road with an uneven profile. The proof is straightforward and is omitted here.

Substituting $z(t) = \phi\eta(t)$ into Eq. (11), rewriting it as $F_c(t) = A^{\mathrm{T}}\tilde{K}\eta(t) - K_{int}S_r r(vt)$, and substituting $\tilde{F}(t) + \tilde{K}\tilde{r}(vt)$ for $\tilde{K}\eta(t)$ into the last equation, we get

$$F_c(t) = A^{\mathrm{T}}\tilde{F}(t) + A^{\mathrm{T}}\tilde{K}AS_r r(vt) - K_{int}S_r r(vt).$$

By virtue of identity (12), it reduces to the simple equation

$$F_c(t) = A^{\mathrm{T}}\tilde{F}(t). \tag{13}$$

The implementation of the above-described decomposition technique for calculating forces acting on the road from an MDOF vehicle is very simple and is summarized as follows.

(1) Solve the eigenvalue problem $(K - \omega^2 M)\phi = 0$ to decouple the MDOF problem.
(2) Calculate the model scaling matrix A by formula (7).
(3) Transform the input $S_r r(x)$ of the original problem into that for the uncoupled problem by means of the matrix A: $\tilde{r}(x) = AS_r r(x)$.
(4) Solve the uncoupled system of equations (9) to get the forces $\tilde{F}$.
(5) Transform these forces to the contact ones by means of the matrix A^{T}: $F_c = A^{\mathrm{T}}\tilde{F}$.

The decomposition of the MDOF model into an aggregate of independent oscillators reduces the amount of computation. This technique can successfully be applied to solving various problems. One of them is briefly discussed in Section 5.3. In this paper, we will consider the application of the above technique to the calculation of contact forces arising after the passage of a local road surface irregularity by an MDOF vehicle. We will extend the results obtained in Ref. [17] for an SDOF moving oscillator to the case of a linear undamped MDOF vehicle model.

3. Effect of a pothole on the dynamics of an MDOF vehicle

3.1. Problem statement

We will consider an isolated irregularity, further referred to as a *pothole*, of the form

$$r(x) = \begin{cases} -\frac{1}{2}a[1 - \cos\frac{2\pi x}{b}], & 0 \leqslant x \leqslant b, \\ 0, & x < 0,\ x > b, \end{cases} \tag{14}$$

where a and $b > 0$ are the pothole "depth" and "width," respectively. A negative value of a corresponds to a bump. As discussed in Ref. [6], this function "is capable of expressing diverse types of irregularities." We set the problem of finding magnitudes of the harmonic components of the contact forces arising after the passage of the pothole (14) as functions of the vehicle speed and the pothole size.

To solve the problem, we will apply the technique discussed in the previous section. Denote by A_i the ith row of the scaling matrix A and by a_{ij} its entries. Consider the ith equation (10). The longitudinal profile for the ith oscillator can be written as

$$\tilde{r}_i(x) = A_i S_r r(x) \equiv a_{i1} r(x - l_1) + \cdots + a_{im} r(x - l_m). \tag{15}$$

As can be seen, the modal representation of the system implies that each oscillator passes m "potholes" (which, generally, may overlap). All these potholes have the same width b but different depths: the depth of the jth pothole passed by the ith oscillator is equal to $\tilde{a}_{ij} = a_{ij}a$.

After the passage of a pothole, the modal forces $\tilde{F}_j$ are harmonic ones. Denote by $|\tilde{F}_j|$ their amplitudes. Expanding the vector of contact forces into the Fourier series,

$$F_c = \sum_{j=1}^{n} C_j \cos(\omega_j t + \varphi_j) \tag{16}$$

and applying Eq. (13), we get the Fourier coefficients as

$$C_j = A_j^{\mathrm{T}} |\tilde{F}_j|. \tag{17}$$

Thus, the problem of determining the dynamic effect of a pothole on an MDOF vehicle reduces to that of finding the amplitude of the force acting on an SDOF oscillator after passing m potholes.

It will be shown later in this section that m potholes of the same length can be replaced by one "equivalent" pothole. Thus, the key point in finding the dynamic effect of a pothole on an MDOF vehicle is to be able to efficiently calculate the magnitude of the contact force arising after passing one pothole by an SDOF oscillator.

3.2. Earlier results for an SDOF oscillator

The effect of a pothole/bump on the dynamics of vibration of an SDOF undamped vehicle model has been examined in Ref. [17]. It was shown that the magnitude of the harmonic contact force acting on the road after passing a pothole is given by

$$F_c = k_0 a \Phi(\gamma), \tag{18}$$

where γ is the dimensionless parameter

$$\gamma = \frac{b\omega_0}{2\pi v} \equiv \frac{bf_0}{v}; \tag{19}$$

ω_0 ($f_0 = \omega_0/2\pi$) and k_0 are the oscillator eigenfrequency and spring coefficient, respectively. The function

$$\Phi(\gamma) = \frac{|\sin \pi\gamma|}{|\gamma^2 - 1|} \tag{20}$$

called the *dynamic amplification factor* for a pothole (see Ref. [17] for detail), is shown in Fig. 3. By means of the dynamic amplification factor, one can immediately estimate the magnitude of the contact force acting on the road from the oscillator after passing the pothole. As can be seen, it linearly depends on the spring stiffness and the pothole depth, and the remaining three parameters (v, b, and ω_0 or f_0) are combined through the function of one variable $\Phi(\gamma)$.

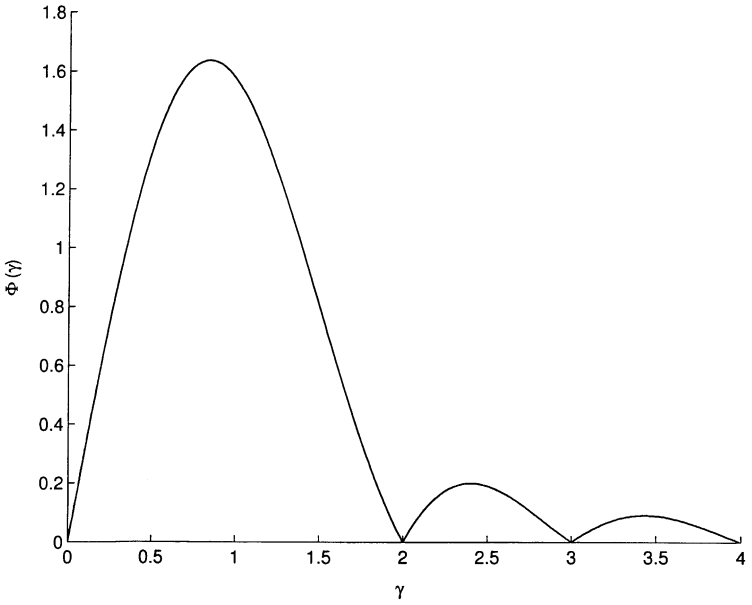

Fig. 3. Pothole dynamic amplification factor $\Phi(\gamma)$.

3.3. An MDOF vehicle with one contact point passing a pothole

We begin the examination of an MDOF vehicle model with the simplest case where a vehicle has one contact point, $m = 1$. In this case, the contact force F_c is a scalar, and A is a vector of length n: $A = [a_{11}, \ldots, a_{n1}]^{\mathrm{T}}$. The jth independent oscillator passes one pothole of width b and depth $\tilde{a}_j = a_{j1}a$, and we can immediately apply the results of Ref. [17] to find amplitudes of the forces $\tilde{F}_j$ by Eq. (18),

$$|\tilde{F}_j| = \tilde{a}_j \tilde{k}_j \Phi(\gamma_j), \tag{21}$$

where $\Phi(\gamma)$ is given by Eq. (20) and

$$\gamma_j = f_j b/v. \tag{22}$$

The Fourier coefficients C_j given by Eq. (17) are calculated analytically as

$$C_j = a_{j1}\tilde{a}_j \tilde{k}_j \Phi(\gamma_j). \tag{23}$$

Thus, given the parameters of the uncoupled system, the function $\Phi(\gamma)$, shown in Fig. 3, bears all required information about the behavior of the MDOF system after passing a pothole.

Note that in the case of an MDOF vehicle, it is more convenient to plot all functions C_j in one figure in order to get a better idea of the contribution of each oscillator to the dynamics of vehicle vibration. These curves can be plotted versus the parameter b/v for a fixed value of the pothole depth a (the dependence on which is trivial).

As an illustration, consider the "quarter-car" model (Fig. 2(a)) with the following parameters: $m_1 = 3.6 \times 10^4$ kg, $m_2 = 2.0 \times 10^3$ kg [7,18], $k_1 = 4 \times 10^6$, $k_2 = 1.2 \times 10^7$ N/m, and $c_1 = c_2 = 0$.

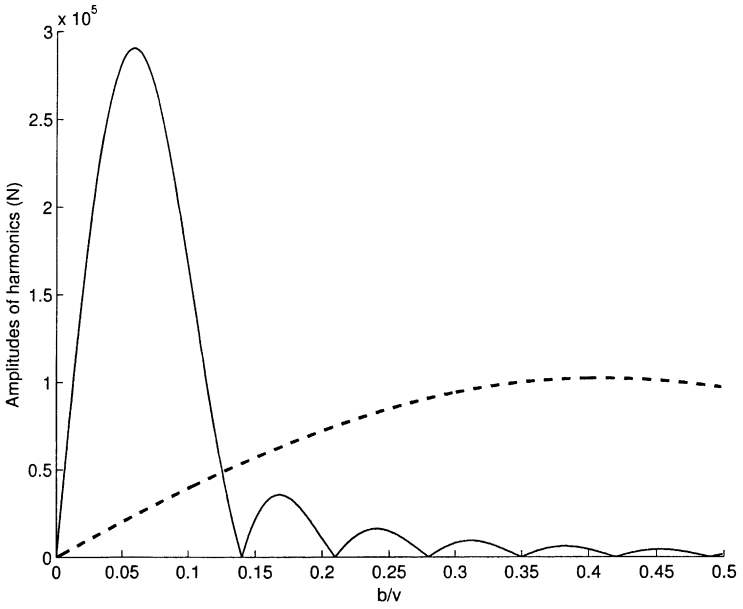

Fig. 4. Amplitudes of the "body-bounce" (dashed line) and "axle-hop" (solid line) forces occurring after traversing the pothole of depth $a = 1$ cm by the 2-DOF ("quarter-car") model.

Applying the technique described in the previous section, we obtain masses and frequencies of the modal oscillators: $\tilde{m}_1 = 3.404 \times 10^4$ kg, $\tilde{m}_2 = 0.403 \times 10^4$ kg, $f_1 = 2.05$ Hz, $f_2 = 14.3$ Hz; and the entries of the scaling matrix A: $a_{11} = 1.05$ and $a_{21} = 0.74$.

Fig. 4 shows dependence of the Fourier coefficients C_1 (dashed line) and C_2 (solid line) of the dynamic contact force acting on the road (vehicle) on the parameter b/v for $a = 1$ cm. As can be seen, for short-wavelength potholes, the high-frequency component (14.3 Hz) associated with the axle-hop vibration is much greater than that due to body-bounce vibration (2.05 Hz), which, in turn, dominates for middle- to long-wavelength potholes (it takes its maximum value when $b/v \approx 0.4$). For example, for $v = 20$ m/s, the largest value of the tire force (about 3×10^5 N) is expected when the pothole width is around 1.2 m ($b/v \approx 0.06$); the peak value of the force associated with the body bounce is about three times less and occurs for $b \approx 8$ m at the same speed.

3.4. General case of an MDOF vehicle

3.4.1. Arbitrary number of contact forces

Let the number of contact points be arbitrary, $m \neq 1$. In this case, F_c is an m vector of contact forces. Since each contact force generally has its own Fourier expansion, the total number of the Fourier coefficients is equal to $m \times n$. The basic difference of this case from the case of one contact point is that each independent oscillator in the modal space passes m, rather than one, potholes. As follows from Eq. (15), all potholes have the same width but different depths.

Let us show that several potholes of identical widths can be replaced by one "equivalent" pothole, which reduces the problem to that considered in the previous section. We consider an oscillator moving along the horizontal rigid surface with m potholes (bumps) as shown in Fig. 5

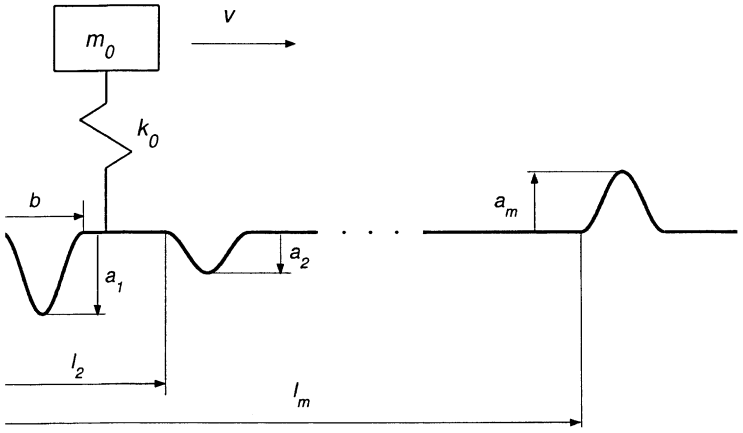

Fig. 5. An SDOF oscillator passing m potholes of the same width b.

and pose the problem of finding the amplitude of the oscillator free vibration after passing all potholes.

The potholes are assumed to be of form (14), have the same width b but different depths a_j, and the jth pothole is located at the distance l_j from the first one. If $l_{j+1} - l_j < b$, the $(j+1)$th and jth potholes overlap.

Theorem 1. *The response of a linear undamped oscillator due to m potholes of width b and depths a_s, $s = 1, \ldots, m$, is equal to that due to one pothole of width b and depth $|\tilde{a}|$, where $\tilde{a}$ is the complex number*

$$\tilde{a} = \sum_{s=1}^{m} a_s \, \mathrm{e}^{-\mathrm{i}\omega_0 l_s / v}. \tag{24}$$

Proof. The equation governing vibration of the oscillator can be written in the form

$$\ddot{z}(t) + \omega_0^2 z(t) = \omega_0^2 \sum_{s=1}^{m} r_s(vt). \tag{25}$$

By the superposition principle, the solution to Eq. (25) can be represented as $z(t) = \sum_{s=1}^{m} z_s(t)$, where $z_s(t)$ is a solution of the equation

$$\ddot{z}_s(t) + \omega_0^2 z_s(t) = \omega_0^2 r_s(vt), \quad s = 1, \ldots, m. \tag{26}$$

Denote by T_s the moment when the oscillator leaves the sth pothole, $T_s = T + l_s/v$, where $T = b/v$. For $t \geqslant T_s$, $r_s(vt) = 0$, and the solution to Eq. (26) represents the free vibration of the oscillator

$$z_s(t) = Z_s \cos(\omega_0(t - T_s) + \varphi_0) \equiv Z_s \mathrm{Re}[\mathrm{e}^{\mathrm{i}(\omega_0(t-T_s)+\varphi_0)}]. \tag{27}$$

It has been proven in Ref. [17] that

$$Z_s = a_s \Phi(\gamma), \tag{28}$$

where γ and $\Phi(\gamma)$ are defined by Eqs. (19) and (20), respectively. The phase angle φ_0 is determined by the oscillator parameters and the pothole width but does not depend on a_s, hence, φ_0 is the same for all $z_s(t)$. When $t \geqslant T_m$, representation (27) is valid for all s and we have

$$z(t) = \sum_{s=1}^{m} Z_s \mathrm{Re}[\mathrm{e}^{\mathrm{i}(\omega_0(t-T)+\varphi_0-\omega_0 l_s/v)}] = \mathrm{Re}\left[\Phi(\gamma)\mathrm{e}^{\mathrm{i}(\omega_0(t-T)+\varphi_0)} \sum_{s=1}^{m} a_s \, \mathrm{e}^{-\mathrm{i}\omega_0 l_s/v}\right]. \tag{29}$$

Then, it follows that the magnitude of the oscillator free vibration after passing m potholes is

$$Z = \left| \sum_{s=1}^{m} a_s \, \mathrm{e}^{-\mathrm{i}\omega_0 l_s/v} \right| \Phi(\gamma). \tag{30}$$

Comparing this with Eq. (28), we get Eq. (24).

Eq. (24) suggests the following way of calculation of the depth of the equivalent pothole. Each of the m potholes is assigned a complex depth by multiplying the real value a_s by $\exp(-\mathrm{i}\omega_0 l_s/v)$, which accounts for the time lag between the passage of the pothole by the sth and first contact points. The depth of the equivalent pothole is then the magnitude of the sum of the complex depths obtained.

By means of Theorem 1, the calculation of the Fourier coefficients reduces to the case considered in Section 3.3. Indeed, given one pothole of depth a in the physical space, the jth oscillator in the modal space passes m potholes of depths $a_{j1}a, \ldots, a_{jm}a$, where a_{ji} are entries of the scaling matrix A (see Eq. (15)), which, by Theorem 1, is equivalent to passing one pothole of depth $|\tilde{a}_j|$ calculated by Eq. (24)

$$\tilde{a}_j = a \sum_{s=1}^{m} a_{js} \, \mathrm{e}^{-\mathrm{i}\omega_j l_s/v}. \tag{31}$$

Then, the modal forces $|\tilde{F}_j|$ are calculated by Eq. (21) with the substitution of $|\tilde{a}_j|$ for $\tilde{a}_j$ and the vector C_j of the Fourier coefficients, by Eq. (17).

Remark 2. The scalar equation (23) obtained for the case of one contact point can be used to calculate components of the vector C_j. The pth component of C_j (the jth Fourier coefficient of the pth contact force) is obtained by substitution of a_{jp} for a_{j1} into (23).

3.4.2. Multiple eigenfrequencies

Finally, we need to consider the case of multiple vehicle eigenfrequencies, which seems to be rather typical for real vehicles. Let $\omega_{j1} = \omega_{j2} = \omega_j$. We have two harmonics with the same frequency in expansion (16), which are to be considered as one harmonic. Thus, we need to find the Fourier coefficient of the harmonic corresponding to the repeated eigenfrequency ω_j. Since the j_1th and j_2th eigenvectors are different, the j_1th and j_2th rows of the matrix A are also different, and, hence, the depths of m potholes passed by two oscillators are generally different. This implies that complex depths of the equivalent potholes for the j_1th and j_2th modal oscillators are different as well, and the oscillator vibrations are generally not in phase such that we cannot simply add two corresponding Fourier coefficients in Eq. (16).

Consider free vibration of the j_1th and j_2th oscillators in the modal space after passing all m potholes. By Eq. (29), we have

$$\eta_{j_k}(t) = \mathrm{Re}[\tilde{a}_{jk} e^{i(\omega_j(t-T)+\varphi_j)}]\Phi(\gamma_j), \quad k = 1, 2,$$

where $\tilde{a}_{jk}$ is complex depth of the "equivalent" pothole for the j_kth modal oscillator given by Eq. (31). The modal forces acting on the road are given by $\tilde{F}_{j_1} = \tilde{k}_{j_1}\eta_{j_1}$ and $\tilde{F}_{j_2} = \tilde{k}_{j_2}\eta_{j_2}$. Transforming them into the physical space by means of Eq. (13) and adding them together, we find the harmonic component of the contact force $F_c(t)$ corresponding to the frequency ω_j,

$$A_{j_1}^{\mathrm{T}}\tilde{F}_{j_1}(t) + A_{j_2}^{\mathrm{T}}\tilde{F}_{j_2}(t) = \mathrm{Re}[(A_{j_1}^{\mathrm{T}}\tilde{k}_{j_1}\tilde{a}_{j_1} + A_{j_2}^{\mathrm{T}}\tilde{k}_{j_2}\tilde{a}_{j_2})\, e^{i(\omega_j(t-T)+\varphi_j)}]\Phi(\gamma_j).$$

Noting that the right-hand side of the last equation represents the harmonic function with the amplitude $|A_{j_1}^{\mathrm{T}}\tilde{k}_{j_1}\tilde{a}_{j_1} + A_{j_2}^{\mathrm{T}}\tilde{k}_{j_2}\tilde{a}_{j_2}|\Phi(\gamma_j)$ and extending this to the case of arbitrary multiplicity of a repeated eigenfrequency, we arrive at the following theorem.

Theorem 2. *If a vehicle eigenfrequency ω_j has multiplicity p such that $\omega_{j_1} = \omega_{j_2} = \cdots = \omega_{j_p} \equiv \omega_j$, the Fourier coefficient of the corresponding harmonic component in the expansion of the contact force is*

$$C_j = |A_{j_1}^{\mathrm{T}}\tilde{k}_{j_1}\tilde{a}_{j_1} + \cdots + A_{j_p}^{\mathrm{T}}\tilde{k}_{j_p}\tilde{a}_{j_p}|\Phi(\gamma_j). \tag{32}$$

The last result implies that the case of repeated eigenfrequencies presents, in fact, almost no additional difficulties. Indeed, in the general case, we simply need to perform all calculations in the complex plane: to find complex depths $\tilde{a}_j$ (rather than only their magnitudes $|\tilde{a}_j|$) for all oscillators in the modal space and to calculate complex Fourier coefficients as $A_j^{\mathrm{T}}\tilde{k}_j\tilde{a}_j\Phi(\gamma_j)$ for all n harmonics (without regard to whether they are single or multiple). Then, if some eigenfrequencies are identical (or close to each other), we add the corresponding complex Fourier coefficients. And only after this, we take absolute values of the Fourier coefficients obtained to get real coefficients of expansion (16).

3.4.3. Algorithm for the general case

Summing up the discussions in this section, we arrive at the following algorithm for calculation of the Fourier coefficients of the expansion of the contact forces arising after passing a pothole (14).

(1) Decompose the vehicle model into an aggregate of independent SDOF oscillators in the modal space to get vehicle eigenfrequencies and eigenfunctions and the real-valued $n \times m$ scaling matrix A.
(2) Calculate complex depths of the equivalent potholes for all modal oscillators by Eq. (31).
(3) Calculate the complex magnitudes of the modal forces by Eq. (21).
(4) Get n complex m-vectors of the Fourier coefficients by Eq. (17).
(5) Check if there are multiple eigenfrequencies. If such eigenfrequencies exist, reduce the number of the coefficients by adding together those that correspond to one repeated eigenfrequency.
(6) Take absolute values of the complex Fourier coefficients obtained.

As a result of this procedure, we get n_d real vector functions $C_j \in \mathbb{R}^m$ of the Fourier coefficients, where n_d is the number of different eigenfrequencies. The rth component of the jth vector is the function showing the dependence of the magnitude of the jth harmonic component of the rth

contact force on the vehicle speed and pothole width. As in the case of one contact force, it is more illustrative to depict all Fourier coefficients corresponding to one contact force in one figure as functions of b/v for a fixed value of the pothole depth a.

The basic difference of the general case from the case of one contact point is that the Fourier coefficients in the former case depend on two parameters rather than on one parameter as it was in the latter case. Indeed, $\Phi(\gamma_j)$ is a function of the ratio b/v, and the depth of the equivalent pothole given by Eq. (31) is a function of vehicle speed v. The shape of each curve C_{jr} plotted versus b/v and the abscissa of its peak depend only on the eigenfrequency of the corresponding oscillator and are determined by the function $\Phi(\gamma_j)$. However, the height of the curve is determined by the $\tilde{a}_j$, which now depends on the speed. Thus, if we want to examine the dependence of the Fourier coefficients on both vehicle speed and pothole width, we have to consider a family of plots parametrized by the values of the vehicle speed. Note that one can choose a different pair of independent parameters, e.g., b and v; however, the pair b/v and v seems to be more convenient.

3.5. Example

To illustrate the technique described in the previous section, we applied it to calculation of the Fourier coefficients of the contact forces arising after passing a pothole of form (14) by the 4-DOF vehicle model with two contact points shown in Fig. 2(b). The values of the masses m_1 and m_2 and the spring coefficients are the same as those considered in Section 3.3, the second order mass moment of inertia $I_1 = 1.44 \times 10^5$ kg m^2 [7], and the distance between axles $l = 3$ m. As in the previous case, the damping was set zero.

Applying the decomposition technique described in Section 2, we find the eigenfrequencies $f_1 = 1.54$, $f_2 = 2.05$, $f_3 = f_4 = 14.3$ Hz. The first and second eigenfrequencies correspond to the pitch and body-bounce vibrations, respectively. The repeated eigenfrequency 14.3 Hz corresponds to two axle-hop vibrations. The scaling matrix A is

$$A = \begin{bmatrix} 0.3827 & -0.3827 \\ 0.5427 & 0.5427 \\ -0.5262 & 0.5262 \\ -0.5229 & -0.5229 \end{bmatrix}.$$

Figs. 6 and 7 show the amplitudes of the pitch (dashed line), body-bounce (bold solid line), and axle-hop (thin solid line) components of the first contact force after passing a pothole of depth $a = 1$ cm versus b/v for two values of the vehicle speed: 10 and 30 m/s, respectively. In view of the model symmetry, the results related to the second contact force are the same and not presented. As can be seen, the Fourier coefficient corresponding to the repeated axle-hop eigenfrequency is not affected by the vehicle speed and depends only on the parameter b/v, whereas the pitch and axle hop do depend on both parameters.

In certain circumstances, e.g., when a road surface is known to have irregularities of a fixed wavelength, it may be advisable to plot the Fourier coefficients as functions of vehicle speed for that value of b in order to be able to determine "dangerous" values of speed, for which the contact forces are especially large. Figs. 8 and 9 show the Fourier coefficients of the first contact force after the passage of the short- and long-wavelength potholes, respectively. As can be seen, the low-

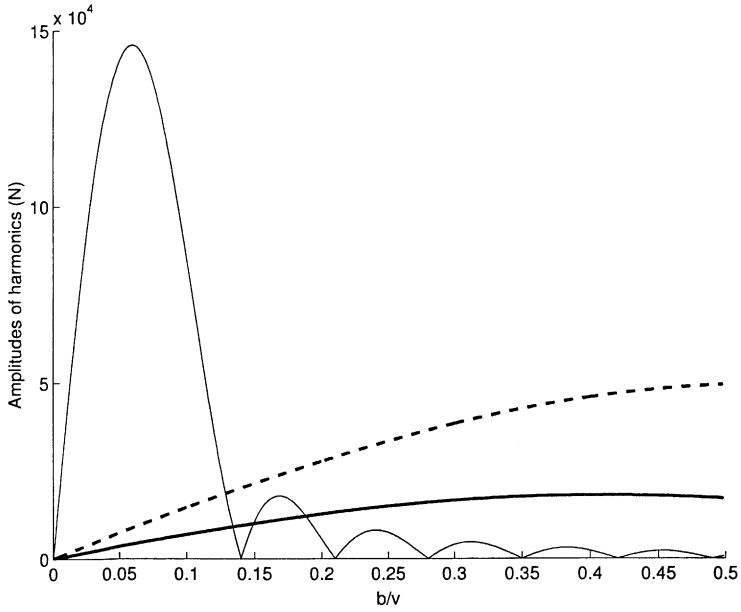

Fig. 6. Amplitudes of the pitch (dashed line), body-bounce (bold line), and axle-hop (thin solid line) components of the first contact force after passing the pothole of depth $a = 1$ cm for the 4-DOF model moving at $v = 10$ m/s.

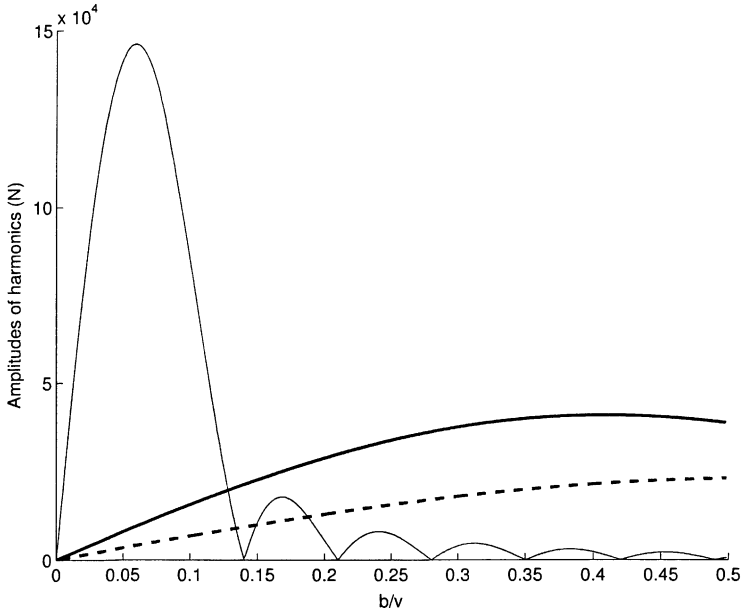

Fig. 7. Amplitudes of the pitch (dashed line), body-bounce (bold line), and axle-hop (thin solid line) components of the first contact force after passing the pothole of depth $a = 1$ cm for the 4-DOF model moving at $v = 30$ m/s.

frequency body-bounce and pitch forces arising after the passage of the short pothole are negligibly small compared to the high-frequency axle-hop force in the whole interval of speed values of interest. On the contrary, in the case of the long pothole, the body-bounce and pitch

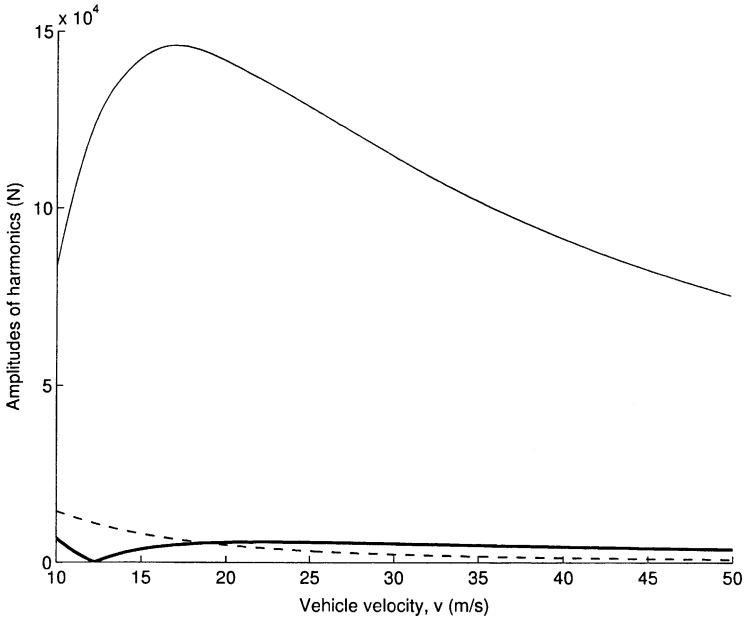

Fig. 8. Dependence of amplitudes of the pitch (dashed line), body-bounce (bold line), and axle-hop (thin solid line) components of the first contact force on vehicle speed for the 4-DOF model after the passage of the "short" pothole of width $b = 1$ m and depth $a = 1$ cm.

forces are considerably greater than the axle-hop force. Fig. 9 also demonstrates that, although the peak values of the body-bounce and pitch forces are almost the same for the given pothole, the contributions of these forces in the total contact force in different intervals of speed are considerably different.

3.6. Another form of representation of the results

There is another way to represent the results, which seems to be more appropriate when we want to examine a wide range of vehicle speeds and to avoid drawing many figures. Indeed, the jth Fourier coefficient can be written in the form

$$C_j(b, v) = A_j^{\mathrm{T}} \tilde{k}_j \tilde{a}_j \Phi(\gamma_j) \equiv \alpha_j(v) \Phi_j(b/v). \tag{33}$$

(Here, $C_j(b, v)$ and $a_j(v)$ are m vectors; however, in the following discussion, we consider Eq. (33) as a scalar equation associated with a certain contact point, in which, for simplicity of notation, the subscript denoting a particular contact point is dropped.) Thus, each Fourier coefficient is obtained from the unique function $\Phi(\gamma)$ by scaling the variable b/v, $\Phi_j(b/v) \equiv \Phi(\gamma_j)$, where $\gamma_j = f_j b/v$, and by multiplying it by the corresponding speed-dependent coefficient $\alpha_j(v) = A_j^{\mathrm{T}} \tilde{k}_j \tilde{a}_j$. Then, instead of drawing figures of the Fourier coefficients for different speeds (or different potholes), we can confine ourselves to two figures: one figure with the plots of the functions $\Phi_j(b/v)$, $j = 1, \ldots, n_d$ and the other with the plots of the multipliers $\alpha_j(v)$. Under such a representation, the first figure shows the shape and relative locations of the curves representing the

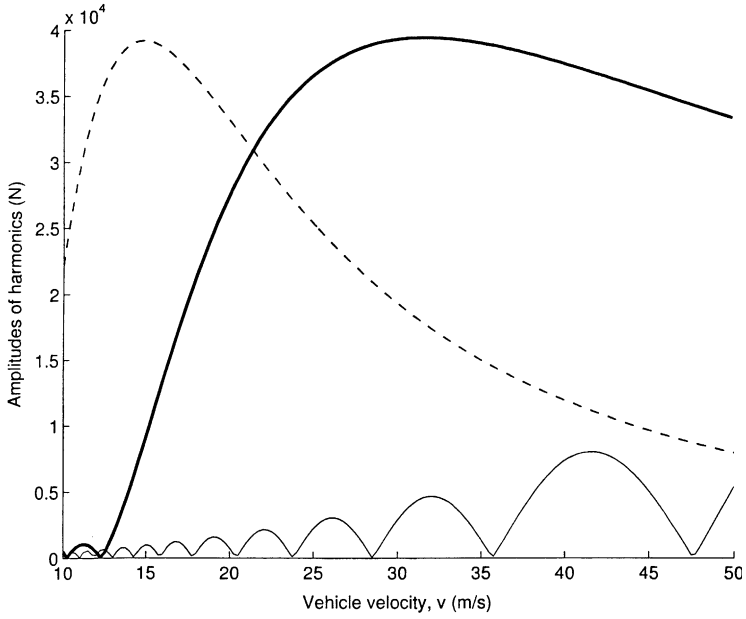

Fig. 9. Dependence of amplitudes of the pitch (dashed line), body-bounce (bold line), and axle-hop (thin solid line) components of the first contact force on vehicle speed for the 4-DOF model after the passage of the "long" pothole of width $b = 10$ m and depth $a = 1$ cm.

Fourier coefficients. In particular, it shows the regions of the parameter b/v where the harmonic forces take their maximum values or, vice versa, can be neglected. The second figure shows dependence of the multipliers α_j on the vehicle speed. The use of both figure allows us to accurately evaluate the Fourier coefficients for any values of the pothole width b and vehicle speed v.

To illustrate the above-said, this way of representation of the results is applied to the "half-car" model considered in Section 3.5. Fig. 10 depicts three dimensionless functions $\Phi_j(b/v)$, which show how the axle-hop, body-bounce, and pitch forces depend on b/v and where they take their maximum values. The dependence of the magnitudes of these forces on the vehicle speed is shown in Fig. 11. As can be seen, the axle hop does not depend on the speed (to be more precise, it depends only on b/v); the dependence of the body-bounce and pitch forces on the speed, known as the "wheelbase filtering" phenomenon (see, e.g., Refs. [12,15,16]), is considerable and cannot be neglected.

4. On one phenomenon reported in the DIVINE report

The DIVINE report [1] defines air suspension as more road-friendly than steel suspension and recommends using it instead of the latter, but notes that "For short-span bridges (10 m) with poor profiles, large dynamic responses occur for both air- and steel-suspended vehicles." By taking into account that the basic difference between two suspensions is in the body-bounce natural

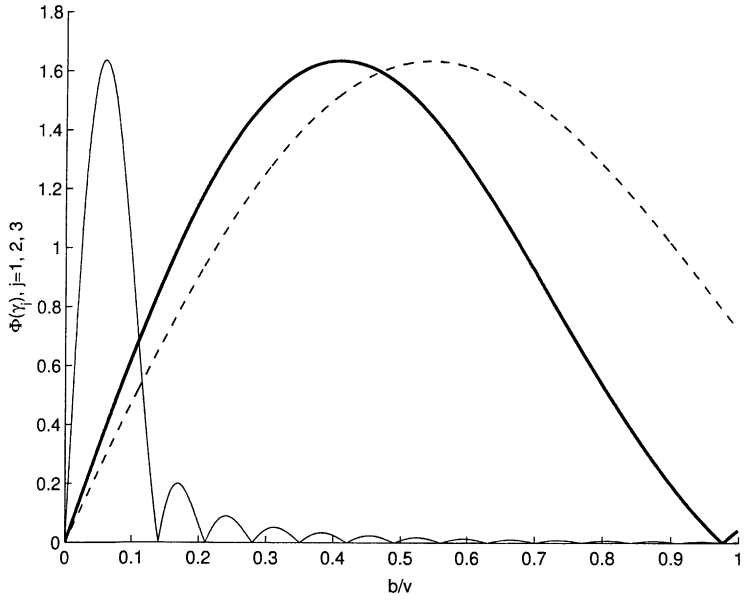

Fig. 10. Functions $\Phi_1(b/v)$ (dashed line), $\Phi_2(b/v)$ (bold line), and $\Phi_3(b/v)$ (thin solid line) for the 4-DOF model.

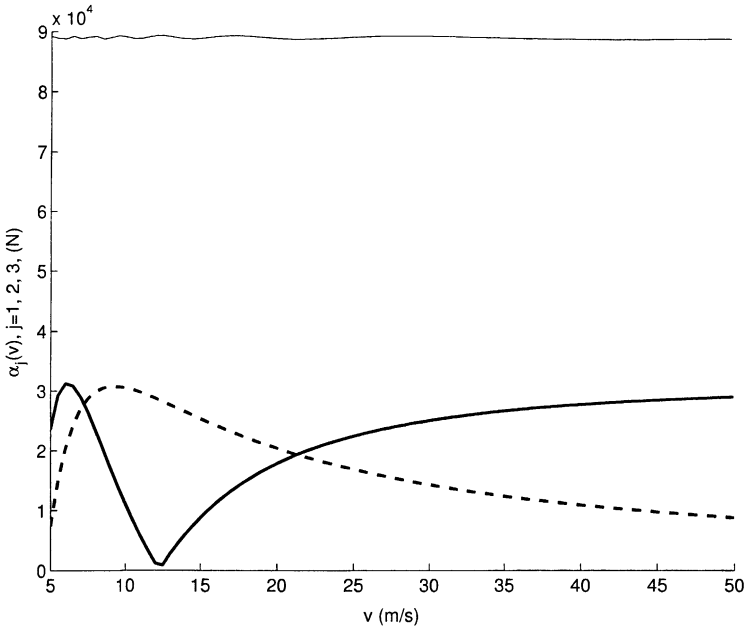

Fig. 11. Magnitudes of the harmonic forces $\alpha_1(v)$ (dashed line), $\alpha_2(v)$ (bold line), and $\alpha_3(v)$ (thin solid line) for the 4-DOF model.

frequencies whereas the vibration of short-span bridges are affected by axle hop (fundamental frequencies of such bridges are in the range of axle-hop frequencies), this observation sounds quite natural.

It is further noted, however, that [1, p. 11] "The highest measured responses were for short-span bridges … traversed by air-suspended vehicles where axle hop was excited by short-wavelength roughness." This observation seems to rely on results of field experiments reported in the work [2], which also states: "Generally the peak bridge deflections were smaller when the air suspensions were fitted except when axle hop was induced by roughness." At first glance, the phenomenon observed in Ref. [2] sounds strange and raises the question: how could softening of the suspension (reduction of the body-bounce frequency) increase the bridge response affected by axle hop? The conclusion of the paper [2] that "vehicles fitted with air suspension can couple with short-span bridges" does not answer the question and explains nothing.

As noted in Ref. [1, p. 53], in the case of short-span bridges, the dynamics of the bridge vehicle system is completely different from that in the case of medium- to long-span bridges, and "true interaction no longer occurs." Under these conditions, the model of a bridge "being forced to vibrate by external forces—i.e., dynamic wheel loads—without taking the vehicle masses into account" should be adopted. Then, in view of matching of the fundamental frequency of the bridge and the axle-hop frequency, the increase in the bridge vibration can be explained by an increase in the axle-hop force. We applied the technique developed in this paper to check whether the replacement of a steel suspension by an air suspension results in an increase in the axle-hop force.

In terms of the 2-DOF model shown in Fig. 2(a) replacement of a steel suspension by an air suspension is modelled by softening the spring k_1 supporting the vehicle body. The other spring k_2 is not changed since we assume that the tires remain the same. Considering the 2-DOF model with the body-bounce frequency 2.05 Hz used in the experiment described in Section 3.3 (Fig. 4) as "steel-suspended," we reduced the spring coefficient k_1 by two times, $k_1 = 2 \times 10^6$ N/m, which, in turn, reduced the body-bounce and axle-hop frequencies to 1.55 and 13.3 Hz, respectively. The modified model was assumed to represent the "air-suspended" vehicle. The masses of the modal oscillators for the "air-suspended" model are $\tilde{m}_1 = 3.53 \times 10^4$ kg and $\tilde{m}_2 = 0.401 \times 10^4$ kg, and the entries of the scaling matrix A are $a_{11} = 1.02$ and $a_{21} = 0.85$. The amplitudes of the body-bounce and axle-hop forces for the "air-suspended" model are depicted in Fig. 12 by the dashed and solid lines, respectively. As could be predicted, the reduction of the suspension frequency considerably reduced the force associated with the body bounce. However, at the same time, this increased the magnitude of the high-frequency force associated with the axle-hop by about 15% (in spite of the fact that the axle-hop frequency diminished!). Since the axle-hop and bridge eigenfrequencies are assumed to match well, the increase of the axle-hop force immediately results in the increase of the bridge response.

Note that the result obtained is not specific to the example considered but is rather general. Softening of vehicle suspension decreases magnitude of the low-frequency force associated with the body bounce but increases the amplitude of the high-frequency axle-hop force. From the physical standpoint this phenomenon can be explained as follows. By softening the suspension spring coefficient, we permit the axle (which vibrates between the road and vehicle body) to vibrate with greater amplitude. Since the force transmitted to the road is determined by the amplitude of the axle vibration and by the spring coefficient k_2, which has not been changed (the tires are the same), its magnitude increases. This implies that an air-suspended vehicle is potentially dangerous for short-span bridges with fundamental frequencies in the range of vehicle axle-hop frequencies. Moreover, although air-suspended vehicles are considered "road-friendly",

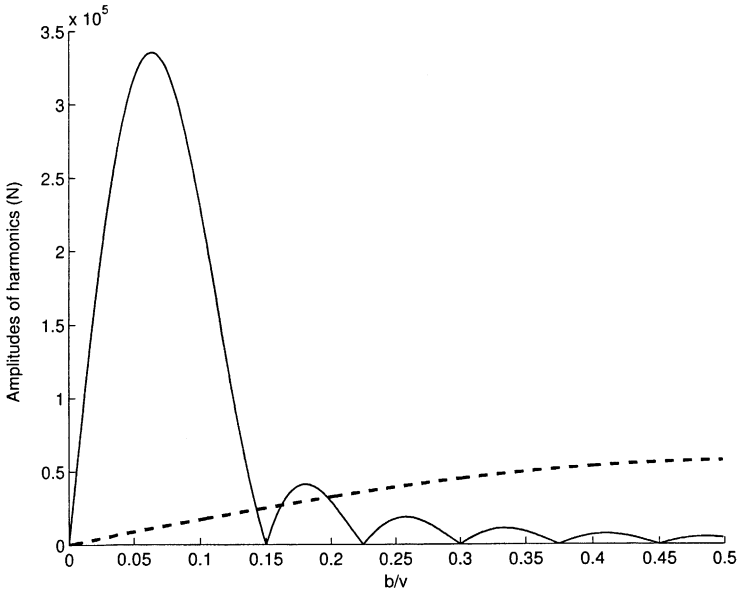

Fig. 12. Amplitudes of the "body-bounce" (dashed line) and "axle-hop" (solid line) forces for the "air-suspended" model.

they can produce a greater pavement damage compared to steel-suspended vehicles in the case of uneven road surface with short-wavelength irregularities, which excite the axle-hope vibration.

We believe that the above explanation of the phenomenon discussed is more realistic (and simpler) than that given in the DIVINE report [1, p. 77]: "A probable explanation for this is the fact that the very limited dynamic load sharing in air suspension allows the axles in a group to vibrate in phase at axle-hop frequencies. 'Cross-talk' between conventional steel leaf suspension limits this possibility."

5. Discussion of possible extensions and applications of the technique

5.1. Other local irregularities

The results discussed in Section 3 are not specific to the pothole described by function (14). We used this particular pothole simply because its dynamic amplification factor, the function $\Phi(\gamma)$, is available in the analytical form [17]. As can be seen, the technique is easily adopted to any other local irregularity if its dynamic amplification factor, which shows the dependence of an SDOF oscillator response on the oscillator and irregularity parameters, can be calculated. The only thing that is required to be done when considering a pothole of a different form is to replace one function $\Phi(\gamma)$ by another. In particular, one can take advantage of the dynamic amplification factor

$$\Phi_s(\gamma) = \frac{4\gamma}{|1 - 4\gamma^2|} |\cos \pi\gamma|$$

given in Ref. [17] to obtain the Fourier coefficients of the contact forces due to passage of a "half-sine" pothole

$$r(x) = \begin{cases} -a \sin \frac{\pi x}{b}, & 0 \leqslant x \leqslant b, \\ 0, & x < 0, x > b \end{cases}$$

(which differs from the "cosine" pothole (14) in that the derivative of $r(x)$ at $x = 0$ and $x = b$ have jumps) by an MDOF vehicle.

If an irregularity can be represented as a linear combination of potholes (14), its dynamic amplification factor can be obtained as a combination of functions $\Phi(\gamma)$ for individual potholes by applying the superposition principle. If all potholes representing the given irregularity have the same width, one can apply the technique used in Section 3.4 and to replace the irregularity by a pothole (14) of variable depth depending on the vehicle speed.

5.2. Damped vehicle models

The key point in the approach suggested is the decomposition of the moving MDOF system into an aggregate of independent moving oscillators. In the undamped case, the governing equations can always be uncoupled by transforming to modal coordinates. In the damped case, this transformation does not uncouple the equations, except for a special case of proportional damping, and we have the two following possibilities.

5.2.1. Approximate decomposition in the modal space

By transforming to the modal co-ordinates using the eigenvectors of the corresponding undamped vehicle model and neglecting the off-diagonal entries of the modal damping matrix, we get an approximate decomposition of the system into an aggregate of independent damped oscillators in the modal space. As in the undamped case, each modal oscillator moves along its own profile, which is determined by means of the same model scaling matrix A, and we have the same Eq. (13) relating physical and modal contact forces. Numerical experiments show that the error of the approximation is not high from the practical standpoint (the system dynamics is determined, in the first turn, by the diagonal elements of the modal damping matrix). The quality of the approximation depends not on the "level of damping" in the system but rather on the "degree of damping nonproportionality" (this notion can be defined in strict terms), such that even a highly damped system can perfectly be approximated in this way.

5.2.2. Exact decomposition in the state space

By introducing the state variables $z(t)$ and $\dot{z}(t)$, the system of n second order differential equations governing vehicle vibration is reduced to a set of $2n$ real state space equations. This system can always be diagonalized, resulting in an uncoupled system of n complex first order differential equations (or $2n$ real equations), which can be solved independently. If a pothole is described by an analytical function, the first order complex differential equation can always be solved analytically resulting in a complex-valued analog of function $\Phi(\gamma)$ (note that the use of complex arithmetic considerably simplifies all analytical calculations, such that the function $\Phi(\gamma)$ can be obtained with much less effort than in the case of a real second order equation).

Both approaches have already been implemented and, at the moment, are under numerical verification. The advantage of the first approach is in its physical clearness. Still, the second approach seems to be more promising since it is exact (no approximations are involved) and because of the convenience of analytical calculations using complex arithmetics.

Note also that, in the damped case, the contact forces are expanded in a series of functions $e^{-\xi_j t}\cos(\omega_j t + \varphi_j)$, where ξ_j is the damping coefficient of the jth modal oscillator. Thus, the Fourier coefficients to be calculated are magnitudes of the exponentially decaying harmonic functions.

5.3. Reduction of vehicle models

In the problems related to bridge vibration, the use of an SDOF vehicle model is often justified in view of the fact that only vehicle vibrations at a frequency close to the bridge fundamental frequency considerably affect the vibration of the bridge. The use of an SDOF vehicle model simplifies the analysis and, thus, is more convenient for the designer. Then, one faces the following problem. Given an MDOF vehicle model and a bridge, what oscillator is to be chosen to adequately represent the vehicle model? The technique developed in Section 2 perfectly suits this goal. In certain circumstances, especially when stress calculations are required, it may be advisable to use a reduced system with more than one degrees of freedom, i.e., to retain some modal oscillators with eigenfrequencies not matching the fundamental frequency of the bridge that produce sizable contact forces for a given road surface profile. The additional information provided by the plots of the Fourier coefficients of the contact forces due to road surface irregularities can be used to create an elaborate reduced vehicle model. A technique for the reduction of an MDOF vehicle model based on the method suggested in this paper is discussed in Ref. [19].

6. Conclusions

(1) The technique for decomposition of an undamped MDOF vehicle model moving along an uneven road has been developed. It reduces the problem of vehicle vibration to finding responses of independent SDOF oscillators, with each oscillator moving along its own profile.
(2) The decomposition technique has been applied to finding the Fourier coefficients of contact forces acting on the road/vehicle after passing an isolated road surface irregularity. For certain typical potholes (bumps), the Fourier coefficients are calculated by analytical formulas and explicitly show dependence of contact forces on the vehicle speed and pothole dimensions. Letting any model parameters (lumped masses or spring coefficients) vary, one can immediately get the new set of the Fourier coefficients corresponding to the modified model and, thus, one can easily observe the effect of the parameter variation on the vehicle dynamics.
(3) The technique discussed has been applied to explain one interesting phenomenon reported in the multinational DIVINE project [1].
(4) The extension of the technique to the case of a damped vehicle and its applications to other problems have been discussed.

Acknowledgements

The authors wish to acknowledge the support of the Civil and Mechanical Systems Division of the National Science Foundation through grant number CMS-9800136.

References

[1] Dynamic Interaction between Vehicles and Infrastructure Experiment (DIVINE), 1998, Technical Report, http://www.oecd.org/pdf/M000014000/M00014819.pdf.
[2] R.J. Heywood, Influence of truck suspensions on the dynamic response of a short span bridge over Cameron's creek, *International Journal of Vehicle Design* 3, Special Series: Heavy Vehicle Systems (1996) 222–239.
[3] J.-W. Kou, J.T. DeWolf, Vibrational behavior of continuous span highway bridge—influencing variables, American Society of Civil Engineers, *Journal of Structural Engineering* 123 (1997) 333–344.
[4] A.V. Pesterev, B. Yang, L.A. Bergman, C.A. Tan, Revisiting the moving force problem, *Journal of Sound and Vibration* 261 (2003) 75–91.
[5] A.S. Nowak, M.M. Szerszen, J. Eom, Dynamic loads on bridges, in: J.M. Ko, Y.L. Xu (Eds.), *Advances in Structural Dynamics* (*Proceedings of the International Conference on Advances in Structural Dynamics*), Vol. 1, Elsevier, Hong Kong, 2000, pp. 407–414.
[6] L. Frýba, *Vibration of Solids and Structures under Moving Loads*, Thomas Telford Ltd., London, 1999.
[7] M.F. Green, D. Cebon, Dynamic response of highway bridges to heavy vehicle loads: theory and experimental validation, *Journal of Sound and Vibration* 170 (1994) 51–78.
[8] G.T. Michaltos, T.G. Konstantakopoulos, Dynamic response of a bridge with surface deck irregularities, *Journal of Vibration and Control* 6 (2000) 667–689.
[9] K. Henchi, M. Fafard, M. Talbot, G. Dhatt, An efficient algorithm for dynamic analysis of bridges under moving vehicles using a coupled modal and physical components approach, *Journal of Sound and Vibration* 212 (1998) 663–683.
[10] Y.-B. Yang, B.-H. Lin, Vehicle–bridge interaction analysis by dynamic condensation method, American Society of Civil Engineers, *Journal of Structural Engineering* 121 (1995) 1636–1643.
[11] X.Q. Zhu, S.S. Law, Dynamic load on continuous multi-lane bridge deck from moving vehicles, *Journal of Sound and Vibration* 251 (2002) 697–716.
[12] T.E.C. Potter, D. Cebon, D.J. Cole, Assessing 'road-friendliness': a review, Proceedings of the Institution of Mechanical Engineers Part D, *Journal of Automobile Engineering* 211 (1997) 455–475.
[13] T.D. Gillespie, S.M. Karamihas, Heavy truck properties significant to pavement damage, in: B.T. Kulakowski (Ed.), *Vehicle–Road Interaction*, American Society for Testing and Materials, Philadelphia, 1994, pp. 52–63.
[14] D.J. Cole, D. Cebon, Truck suspension design to minimize road damage, Proceedings of the Institution of Mechanical Engineers Part D, *Journal of Automobile Engineering* 210 (1996) 95–107.
[15] T.D. Gillespie, Heavy Truck Ridde, SAE Special Publication SP 607, 1985.
[16] D.J. Cole, Fundamental issues in suspension design for heavy road vehicles, *Vehicle System Dynamics* 35 (2001) 319–360.
[17] A.V. Pesterev, L.A. Bergman, C.A. Tan, Pothole-induced contact forces in a simple vehicle model, *Journal of Sound and Vibration* 256 (2002) 565–572.
[18] P. Omenzetter, Y. Fujino, Interaction of non-conservative 1D continuum and moving MDOF oscillator, American Society of Civil Engineers, *Journal of Engineering Mechanics* 127 (2001) 1082–1088.
[19] A.V. Pesterev, L.A. Bergman, C.A. Tan, Accurate model reduction in problems of bridge vibration due to moving vehicle, XXX Summer School in Advanced Problems in Mechanics, St. Petersburg, 27 June – 6 July 2002, in press.